Chem. Senses 25: 155–165, 2000

# Analysis of the Molecular Basis for Octanal Interactions in the Expressed Rat I7 Olfactory Receptor

**Michael S. Singer**

Section of Neurobiology and Center for Medical Informatics, Yale University School of Medicine, 236 FMB, 333 Cedar Street, New Haven, CT 06520, USA

*Correspondence to be sent to: Michael Singer, Section of Neurobiology, Yale University School of Medicine, 236 FMB, 333 Cedar Street, New Haven, CT 06520, USA. e-mail: mike@habibi.med.yale.edu*

## Abstract

Expression studies have shown that the rat I7 olfactory receptor (OR-I7) responds preferentially to the aldehyde *n*-octanal. We wished to predict which residues in OR-I7 bind octanal and how the biophysical properties of these residues determine the receptor's odor selectivity. Building on our previous work on aldehyde interactions in olfactory receptors, we constructed a molecular model of OR-I7 based on the 7.5 Å resolution three-dimensional map of rhodopsin. Octanal was automatically docked in the model. The results predicted an odor-binding pocket ~10 Å from the extracellular surface, in a location similar to the epinephrine-binding pocket of the beta-adrenergic receptor and the odor-binding pocket of a previous olfactory receptor model. A lysine on TM4 and an aspartate on TM5 interacted with the aldehyde moiety of octanal. Hydrophobic residues formed Van der Waals contacts with the hydrocarbon portion of octanal. We docked related odor compounds and found that the predicted affinities compared favorably with experimental results. We also tested a number of amino acid substitutions in order to predict their effects on octanal affinity and provide leads for future experimental work.

## Introduction

A critical question for understanding the neural basis of odor discrimination is how odor molecules interact with olfactory receptor proteins. When these receptors were first identified, Buck and Axel (Buck and Axel, 1991) cited sequence diversity in transmembrane domains (TMs) 4 and 5 as evidence that those domains bind odors. This hypothesis was tested and supported by molecular models and sequence analysis, which further predicted an odor-binding pocket composed of specific residues in TMs 3–6 (Singer and Shepherd, 1994; Bajgrowicz and Broger, 1995; Singer *et al*., 1995, 1996; Pilpel and Lancet, 1999). A lead in the analysis of the predicted binding pocket was the identification of two histidines common on TM4, which are hypothesized to bind aldehyde groups (Singer *et al*., 1995; Singer and Shepherd, 1997).

A new opportunity to study aldehyde interactions has come from functional studies (Zhao *et al*., 1998; Krautwurst *et al*., 1998), which have shown that the rat I7 olfactory receptor—OR-I7 (Buck and Axel, 1991)—responds preferentially to the aldehyde *n*-octanal. We are now in a position to analyse OR-I7 in the same way that other members of the G protein-coupled receptor (GPCR) superfamily, such as the β-adrenergic receptor (BAR), have been studied (Strader *et al*., 1989). Even in the absence of a crystal structure, BAR and its interactions with agonist ligands have been well described by a combination of ligand binding, site-directed mutagenesis and molecular modelling studies. To replicate this approach for OR-I7, we have built a molecular model of the receptor and tested interactions with octanal and related odor compounds. The principal questions we wished to address were which residues in OR-I7 bind octanal, and how the biophysical properties of these residues determine the receptor's ligand selectivity. We also wished to test amino acid substitutions in order to provide leads for future experiments.

This paper reports the first model for OR-I7 and builds on our previous work on the OR5 receptor (Singer and Shepherd, 1994), with a number of substantive improvements. For the current model we have taken advantage of the recent three-dimensional map of rhodopsin at 7.5 Å resolution (Schertler, 1998). A member of the GPCR superfamily, rhodopsin represents a clear improvement over the bacteriorhodopsin template on which previous models were based (Schertler, 1998; Rivkees *et al*., 1999; Salminen *et al*., 1999). Another development in the current model is that TM boundaries and rotations were constrained by hydrophobicity data from multiple olfactory receptor sequences. This synthesis of information from multiple sequences provides a firmer biophysical basis for the modelling procedure and obviates the need for homology modelling. We tested the accuracy of this approach on bacteriorhodopsin, a 7TM protein of known structure, and found

© Oxford University Press 2000

that the resulting molecular model closely approximated the crystal structure. We have also implemented more advanced methods of structure refinement, such as molecular dynamics simulations. Finally, we have taken an approach to ligand docking that allows conformational flexibility in the ligand as well as selected receptor side chains.

The results identify a potential binding pocket for octanal that shares features with the binding pocket for epinephrine in BAR (Strader *et al*., 1989) and the odor-binding pocket predicted for OR5 (Singer and Shepherd, 1994; Bajgrowicz and Broger, 1995). We identify two prominent residues in the binding pocket—a lysine and an aspartate—that may play roles in aldehyde selectivity. We also compare ligand affinities from the model with odor responses measured in functional studies and show that the model reproduced most of the experimental results. Finally, we propose targets for site-directed mutagenesis and predict the outcomes of those mutations.

## Materials and methods

To build the OR-I7 model we followed the approach outlined by Cronet *et al*. (Cronet *et al*., 1993), with steps as listed in Table 1. These steps, which start with individual canonical α-helices and then assemble and position these helices, simulate the hypothesized steps of membrane protein folding (Chothia *et al*., 1977; Popot and Engelman, 1990).

### Hydrophobicity profiles

TMs were identified on the basis of hydrophobicity by the multisequence profile method (Donnelly *et al*., 1994), implemented in PERSCAN. A window size of 21 residues was used. The input sequences were 17 full-length rat and canine ORs known to be expressed in olfactory epithelium. Rat sequences included: OR-I7, F3, F5, F6, F12, I3, I8, I9, I14 and I15 (Buck and Axel, 1991), OR5 (Raming *et al*., 1993), and olp4 (Gat *et al*., 1994). Canine sequences included: DTMT (Parmentier *et al*., 1992), and CfOLF1, CfOLF2, CfOLF3 and CfOLF4 (Issel-Tarver and Rine, 1996). For validation, the analysis was repeated on 21 rat olfactory receptors reported by Singer *et al*. (Singer *et al*., 1998). Sequences were aligned by the iterative profile alignment utility of WHAT IF (Vriend, 1990).

Table 2 shows the TM sequences determined from the hydrophobicity profile and used for the OR-I7 model. Analysis of the rat sequences of Singer *et al*. (Singer *et al*., 1998) yielded similar results. With minor variations, the predicted boundaries matched those identified by Buck and Axel (Buck and Axel, 1991). The boundaries shown here are further supported by conserved prolines and charged residues which frequently flank TM boundaries. These amino acids flank all of the predicted TMs, with the exception of the TM3 amino-terminal boundary.

**Table 1** Steps in model construction

| Parameter | Method of determination | Method of validation |
|---|---|---|
| 1. TM boundaries | hydrophobicity profiles | prolines and charged residues |
| 2. TM secondary structure | canonical α-helices | hydrophobicity moments |
| 3. Side-chain rotamers | library search | minimization and dynamics |
| 4. Helix packing | rhodopsin map | GPCR mutagenesis data |
| 5. Helix rotation | hydrophobicity moments | GPCR mutagenesis data |
| 6. Structure refinement | minimization and dynamics | |

**Table 2** Predicted transmembrane domain sequences for OR-I7

| | |
|---|---|
| TM1 | VLLFFLSLLAYVLVLTENMLIIIAI |
| TM2 | PMYFFLANMSFLEIWYVTVTIP |
| TM3 | QLYFFLGLCCTECVLLAVMAYDRY |
| TM4 | LCVQMAAGSWAGGFGISMVKVFLIS |
| TM5 | LTDFVLAIFILLGPLSVTGASYM |
| TM6 | KAFSTCASHLTVVIIFYAASIFIYA |
| TM7 | LVSVLYAVIVPLFNPIIYCLR |

### Canonical helix construction

The sequences from Table 2 were used to build canonical right-handed α-helices with Builder and Homology software (MSI). Side-chain rotamers were searched automatically from a rotamer library (Ponder and Richards, 1987). Helices were then individually energy minimized with Discover (MSI). To simulate membrane conditions, the dielectric constant was set at 1.00. Minimization was carried out for 500 iterations of steepest descents with the consistent variable forcefield (CVFF).

### Helix assembly

The minimized helices were packed into an assembly with Insight II (MSI), based on helical axes resolved from the 7.5 Å three-dimensional map of rhodopsin (Schertler, 1998). This established $x$ and $y$ coordinates as well as tilt for each helix. Helical $z$-coordinates were set such that the midpoint of each helical axis was positioned in the same $z$-plane of the assembly. An important difference between this model and the OR5 model (Singer *et al*., 1994) is that rhodopsin rather than bacteriorhodopsin was used as a template. Schertler (Schertler, 1998) has compared the bacteriorhodopsin and rhodopsin density maps in detail. Salminen *et al*. (Salminen *et al*., 1999) and Rivkees *et al*. (Rivkees *et al*., 1999) recently built rhodopsin-based models

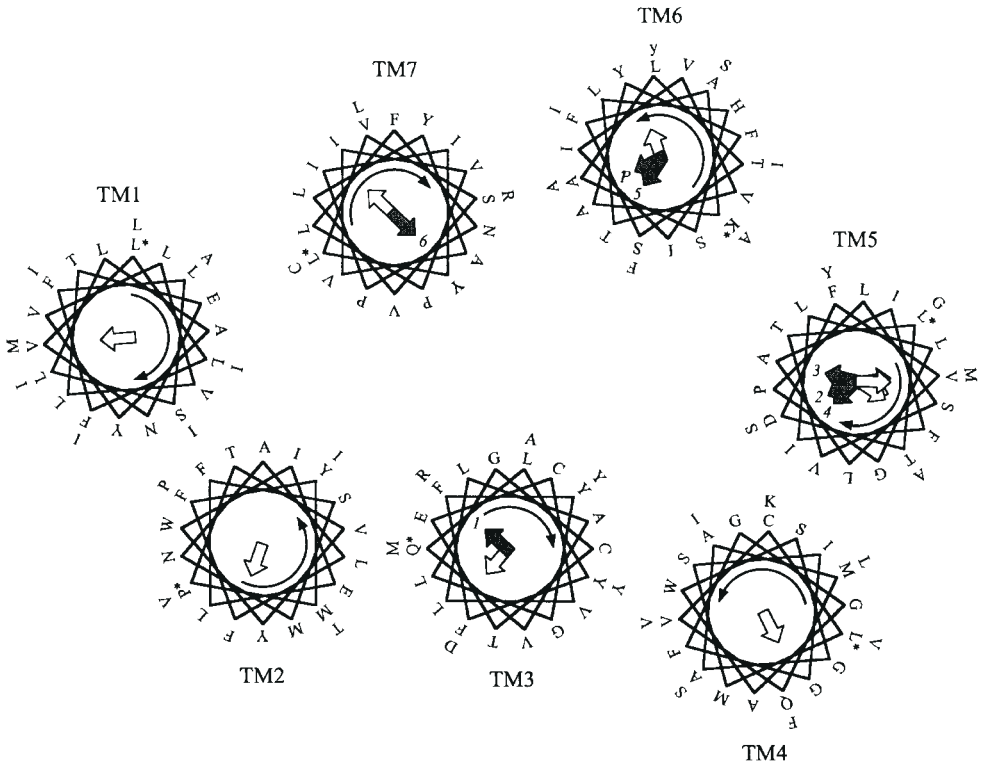


**Figure 1** Helical rotation results, derived from PERSCAN (Donnelly *et al*., 1994). The domains are shown in cross-section ~10 Å below the extracellular surface, as viewed from the extracellular side. Asterisks indicate the first residue in each domain and curved arrows indicate amino–carboxy polarity. Note that the locations of out-of-plane residues may be distorted because of helix tilt. Open arrows inside each helix indicate the hydrophobic moment(s). Moments for TM5 were predicted from four independent samples. Filled arrows indicate residues in other GPCRs shown to face inward by experiment: (1) conserved aspartate in cationic amine receptors (Strader *et al*., 1989); (2) critical threonine in the $m_3$ muscarinic receptor (Wess *et al*., 1991); (3) and (4) two critical serines in the BAR (Strader *et al*., 1989); (5) phenylalanine in BAR that interacts with the aromatic ring of epinephrine (Strader *et al*., 1989); (6) lysine in rhodopsin that covalently binds retinal. (P) Positive selection moments independently predicted the same TM6 helical rotation as that in the OR-I7 model (Singer *et al*., 1996).

of the α-2 adrenergic receptor and A1 adenosine receptor, respectively. The models both successfully predicted results from site-directed mutagenesis, alkylation and ligand-binding studies. Salminen *et al*. (Salminen *et al*., 1999) constructed rhodopsin-based and bacteriorhodopsin-based models in parallel and found that rhodopsin-based model predicted experimental results more accurately. Their report reflects the current consensus in the field that the rhodopsin template is most suitable for GPCR models.

The resolution of the three-dimensional rhodopsin map is 7.5 Å. However, we expect the axes to be more accurate as they were derived from 33 contour cross-sections spaced 2 Å apart (Herzyk and Hubbard, 1998). The interhelical distances, which in our model allow for surface contacts but do not appear to contribute to steric overlap, further support the helical axes.

The transmembrane domains of rhodopsin show ~20% amino acid identity and 50–60% similarity to OR-I7 (results depend on the alignment used). Because tertiary structure remains more conserved than primary structure (Sander and Schneider, 1991), the OR-I7 helical axes are probably similar to those of rhodopsin. The success of adenosine and adrenergic receptor models based on rhodopsin supports this notion (Rivkees *et al*., 1999; Salminen *et al*., 1999). We also tested this point in two transmembrane protein structures from the Protein Data Bank (PDB): photosynthetic reaction centers from two bacterial species, *Rhodopseudomonas viridis* (1PRC) (Deisenhofer and Michel, 1989) and *Rhodobacter sphaeroides* (1AIJ) (Stowell *et al*., 1997) show only 60% overall amino acid similarity, but their helical axes show nearly complete overlap. We conclude that the rhodopsin helical axes provide a valid template for olfactory receptor models.

### Hydrophobicity moments

Helical rotations were predicted by the well-established Fourier transform method (Donnelly *et al*., 1994). For the model, each helix was rotated such that its hydrophobic moment pointed directly away from the assembly. Fourier transforms of hydrophobicity in each domain showed maximum power spectrum values at 100°, indicative of α-helical secondary structure. This supported the identification of these domains as TM helices. Figure 1 shows the helical orientation results and compares them with experimental

data. Previous sequence analysis and molecular model results further supported the helical orientations (see Figure 1).

### Validation on bacteriorhodopsin

To test the validity of the hydrophobicity profiles, canonical helix construction, helix assembly and hydrophobicity moments, we repeated these procedures on bacteriorhodopsin. We did not consult atomic coordinates, only helical axis information from the 2BRD structure (Grigorieff *et al.*, 1996). Transmembrane domains and rotations were predicted from bacterial sensory rhodopsin sequences from the 2BRD entry in the HSSP database (Sander and Schneider, 1991). When the final model (not shown) was compared with the crystal structure, an α-carbon RMS deviation of only 3.15 Å was observed, which is within the 3.50 Å resolution of the crystal structure. This result provides added confidence in the validity of the methods.

### Minimization and dynamics

The helical assembly was minimized with Discover (MSI) for 1000 iterations by steepest descents with CVFF. To simulate membrane constraints, the α-carbon trace was fixed and the dielectric was set at 1.00. Side-chain conformations were explored with 20 ps of molecular dynamics (Discover, MSI). The temperature was 300 K, equilibration time was 100 fs and timestep was 1 fs. The final structure was refined with 1000 iterations of steepest descent minimization, as above.

### Ligand docking

Ligand docking was carried out by a multi-stage process as follows.

#### *Stage 1*

This stage involved search of intermolecular energies with a grid (resolution 0.67 Å), calculated by the Docking module (MSI). Three constraints were placed on Stage 1 docking: first, the ligand was kept in its minimum energy conformation, with all torsions in the *anti* configuration; second, the ligand was only allowed to approach the receptor from the extracellular side; and third, the ligand was not allowed to bind the membrane-exposed portion of the receptor. With the above constraints, octanal was initially positioned above the receptor with the aldehyde oriented downward and was translated and rotated into an energy minimum with the receptor. The process was repeated several times with similar results. Electrostatic interactions with the carbonyl moiety of octanal were the predominant forces at this stage.

An important development for this model was the introduction of flexible ligand docking. The aliphatic portion of octanal has considerable conformational freedom, and flexible receptor side chains were also desirable in order to accommodate the flexible ligand. Stages 2–4 provided the necessary flexible docking methods.

#### *Stage 2*

Automatic docking was carried out with the Affinity module (MSI). For each trial the ligand was automatically moved ≤5 Å in any direction and rotated ≤180° on any axis. Ligand position, conformation, and receptor side-chain conformations were then energy minimized for 500 iterations by the Polak–Ribiere conjugate gradient method. Residues 160, 161, 164, 204 and 251 were allowed to be flexible during the simulation, on the basis that they were predicted to bind odor ligands by previous correlated mutation analysis (CMA) (Singer *et al.*, 1995). Also, torsions between carbons C3 and C4, C4 and C5, C5 and C6, and C6 and C7 on the ligand were allowed to rotate freely. Intermolecular energies, both electrostatic and Van der Waals, were monitored with the Docking module (MSI). We ran 200 trials, chose the five minimum intermolecular energy structures, and submitted these to the next stage.

#### *Stage 3*

This consisted of 20 ps of molecular dynamics as described above.

#### *Stage 4*

The minimum intermolecular energy structure from Stage 3 was minimized for 1000 iterations of steepest descents with backbone fixed and other parameters as above to yield the final OR-I7–octanal complex.

### Responses to different ligands

Octanal was modified in the Stage 3 structure to create the analogs *trans*-2-*n*-octenal, *n*-hexanal, *n*-heptanal, *n*-nonanal, *n*-decanal, *n*-undecanal, *n*-octane, *n*-octanol, 1-fluoro-*n*-octane, and *n*-octanoic acid. Because the substituted ligands were structurally similar to octanal and differed only in their number of carbons, presence of a double bond, or terminal functional group, the complexes were submitted to Stage 4 minimization without further dynamics. Intermolecular energies were evaluated as above and relative affinities were then calculated. These calculations were possible because entropy and solvation enthalpy terms are expected to remain approximately constant for the ligands tested (with some differences in solvation), leaving intermolecular enthalpy as the most important variable term in relative free energy between ligand and receptor.

### Residue substitutions

In order to provide leads for future site-directed mutagenesis experiments, single amino acids were substituted in the appropriate Stage 4 structures. The complexes were reminimized for 1000 iterations and relative intermolecular affinities were estimated as above.

## Results

We will first describe the location of the octanal binding pocket in the OR-I7 model, then focus on critical amino

acids in the pocket. We will then describe the responses to different odor compounds and finally the effects of residue substitutions in the OR-I7 model.

### Octanal binding pocket

After automated docking as described in Materials and methods, we found that octanal bound OR-I7 in a pocket ~10 Å from the extracellular surface and formed by transmembrane domains 3–7. This is similar in location to the epinephrine binding pocket of the BAR (Strader *et al*., 1989) and the odor-binding pocket in the OR5 olfactory receptor model (Singer and Shepherd, 1994). Dynamics archives showed that the carbonyl group of octanal played a pivotal role in the docking process, due to the importance and relatively long-range consequences of electrostatic forces in the low-dielectric milieu. Table 3 lists seven residues that formed the strongest noncovalent interactions with octanal in the final model. The spatial layout of these residues with octanal is summarized in Figures 2 and 3. Lysine 164 and aspartate 204 were the most critical residues in the model. Both had been predicted to bind odor ligands by previous correlated mutation analysis (CMA) of OR-I7 and other rat olfactory receptors (Singer *et al*., 1995). The results thus support previous studies providing evidence that odor ligands interact with olfactory receptors in a binding pocket, and that this binding pocket is similar in location to that found in the BAR.

### Critical residues in the binding pocket

We begin with residues that contributed to electrostatic forces in the model. The positively charged lysine 164 accounted for most of the affinity of OR-I7 for octanal (see Figure 2). This lysine is special in its ability to form an imine bond with octanal to yield a Schiff base. In rhodopsin, a lysine in TM7 forms a Schiff base with the retinal chromophore (Nakayama and Khorana, 1991). Formation of a Schiff base would confer special properties to OR-I7, such as increased affinity for aldehydes and desensitization with slow recovery.

The negatively charged aspartate 204 was also an important component of the binding pocket, but repelled rather than attracted octanal. This residue also competed with octanal for electrostatic interactions with lysine 164 (see Figures 2 and 3). Dynamics archives show that as a result, aspartate 204 immobilized the lysine and limited its interactions with octanal. This may indicate that aspartate prevents octanal from binding the receptor too avidly. Alternatively, the aldehyde may be necessary to stabilize a Schiff base (see above). This motif is present in rhodopsin, where retinal forms a protonated Schiff base with a lysine residue on TM7, and a glutamate on TM3 serves as a counterion (Sakmar *et al*., 1989; Nakayama and Khorana, 1991).

The remaining five residues in the binding pocket formed Van der Waals interactions, mostly with the hydrocarbon portion of octanal. Consistent with this role, most of these residues were hydrophobic. Phenylalanine 262 showed induced fit during docking Stages 3 and 4, closing around the pore that provided access to the pocket in Stages 1 and 2. In dynamics simulations this phenylalanine moved away easily, which would allow the ligand to dissociate from the binding pocket.

**Table 3** Residues that interacted with octanal

| OR-I7 no. | Consensus no. | TM | Importance |
|---|---|---|---|
| Lys164[b] | 430 | 4 | A+++++ |
| Phe262 | 633 | 6 | A+++ |
| Asp204[a,b] | 509 | 5 | R+++ |
| Phe205 | 510 | 5 | A++ |
| Ala258 | 629 | 6 | A++ |
| Ala208[a,b] | 513 | 5 | A+ |
| Val281 | 710 | 7 | A+ |

A = attractive force; R = repulsive force.

[a]Shown to bind ligand in other G protein-coupled receptors.

[b]Predicted to bind odors in independent computational studies.

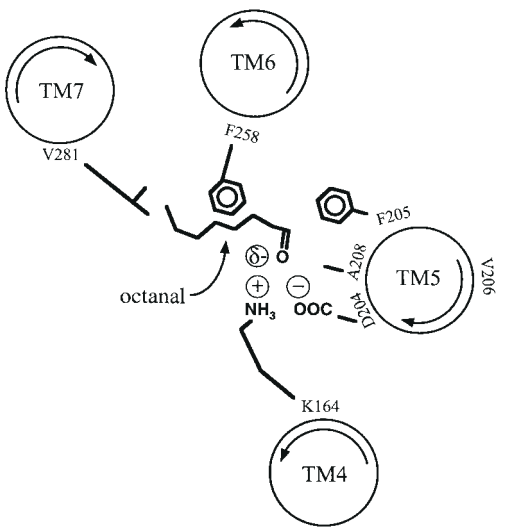


**Figure 2** The predicted octanal binding pocket, viewed *en face* from outside the cell. The predicted position of valine 206 is also indicated on TM5. Curved arrows inside each domain indicate amino–carboxy polarity. (δ–) Negative dipole on the carbonyl croup of octanal; (+) indicates the positive charge on lysine 164; (–) indicates the negative charge on aspartate 204. Helix tilt causes minor distortions in this view. See Figure 3 for additional views.

### Responses to different ligands

We now discuss the binding of other ligands in the OR-I7 receptor model (Table 4). The relative affinity of octanal for OR-I7 is expressed as 1.0000, with the relative affinities of other ligand–receptor complexes expressed on that scale. A monounsaturated analog of octanal, *trans*-2-octenal, had an

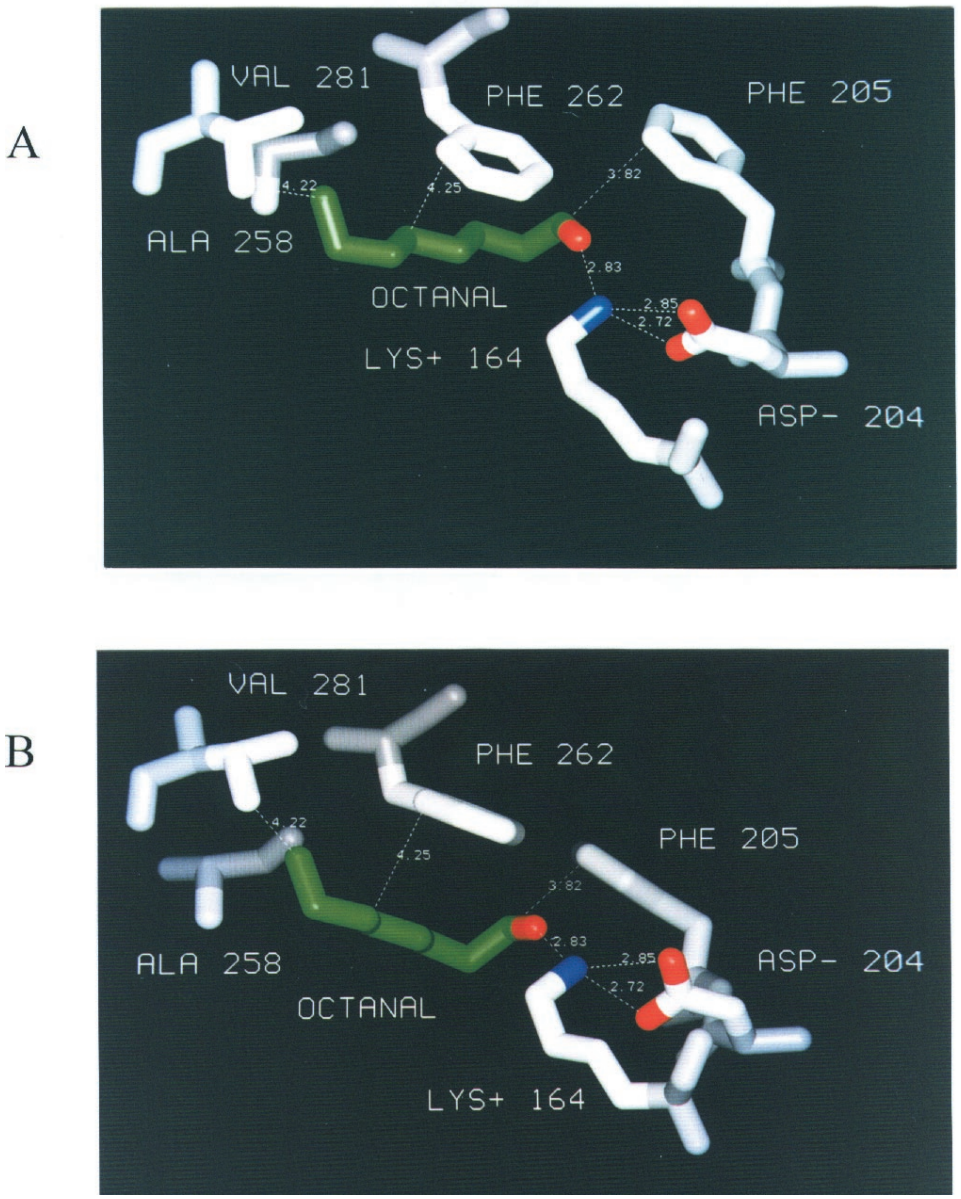


**Figure 3** **(A)** and **(B)** Details from the OR-I7 model showing octanal in the predicted odor-binding pocket. White indicates carbon atoms, red indicates oxygen and blue indicates nitrogen. Green indicates the carbon atoms of octanal. Dotted lines mark distances (Å) between atoms of interest.

affinity for OR-I7 comparable to that of octanal. For the series of *n*-aldehydes from hexanal to undecanal, the model predicted affinities that qualitatively correlated well with experimental results. The correspondence between the model and experimental data for this carbon series is depicted in Figure 4. We did not expect the relation between the predicted affinity and the electro-olfactogram (EOG) amplitude in the experiments of Zhao *et al.* (Zhao *et al.*, 1998) to be a simple linear one, due to the multiple amplification stages leading from the G protein cascade to the EOG response, and the imprecision inherent in both molecular models and EOG recordings. The most important aspect of the results is that both the EOG and model show a maximal response to octanal, with diminishing responses to compounds with fewer or more carbons.

We also tested several analogs that differed only in their terminal functional groups. These results compared favorably with experimental results in that none of the compounds showed an affinity similar to that of octanal. For example, a relative affinity of 0.07 was observed for *n*-octanoic acid. The difference between octanal and octanoic acid appears to stem from electrostatic repulsion by aspartate 204, which is more pronounced for octanoic acid than for octanal. This suggests a novel hypothesis in which

**Table 4** Ligand substitution results

| Ligand | Ligand class | Predicted affinity | Activity by experiment |
|---|---|---|---|
| *n*-Octanal (C8) | aldehyde | 1 | maximal |
| *trans*-2-*n*-Octenal | aldehyde | 0.8 | |
| *n*-Hexanal (C6) | aldehyde | 0.004 | none |
| *n*-Heptanal (C7) | aldehyde | 0.04 | moderate |
| *n*-Nonanal (C9) | aldehyde | 0.3 | moderate |
| *n*-Decanal (C10) | aldehyde | 0.03 | moderate |
| *n*-Undecanal (C11) | aldehyde | <0.0001 | none |
| *n*-Octanoic acid | carboxylate | 0.07 | none |
| 1-Fluoro-*n*-octane | fluorocarbon | 0.02 | |
| 1-*n*-Octanol | alcohol | 0.006 | none |
| *n*-Octane | alkane | <0.0001 | none |

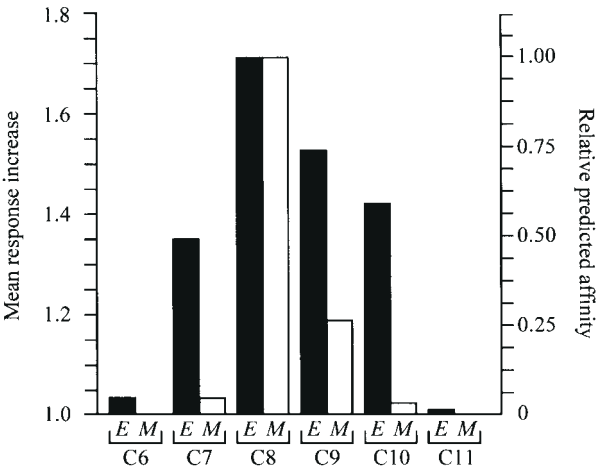


**Figure 4** Comparison of experimentally determined responses (filled bars) and predicted affinities (open bars) for a series of *n*-aldehydes from hexanal (C6) to undecanal (C11). E = experimental result, M = model result. Experimental data are from Zhao *et al*. (Zhao *et al*., 1998). Note the nonlinear relation between the model and experimental results. Both result sets show the same rank-order responses.

aspartate 204 determines odor specificity by means of selective repulsion. The low affinity of 1-fluoro-*n*-octanal in the model could be identified as weaker electrostatic interactions due to the smaller dipole on the fluoro group as compared with the carbonyl of octanal. Despite these observations, the estimated affinities for *n*-octanoic acid and 1-fluoro-*n*-octanal were such that high concentrations of these compounds would be predicted to stimulate OR-I7. Compared to octanal, *n*-octane had almost no affinity for the OR-I7 model. This observation reflects the importance of the aldehyde group present in octanal but lacking in octane. Finally, 1-*n*-octanol had a low affinity for OR-I7, a consequence of the lower dipole on the hydroxyl group as well as interference from the positive dipole of the hydrogen atom.

### Effects of residue substitutions

As a complementary approach to docking different ligands, we carried out two types of mutations in the OR-I7 model. First, we substituted alanine for the critical lysine 164 or aspartate 204 residue (see above) and recorded effects on ligand affinity. Second, we modelled the V206I mutation performed by Krautwurst *et al*. (Krautwurst *et al*., 1998). The results are presented in Table 5.

When alanine was substituted for lysine 164 (K164A), predicted ligand–receptor affinity declined by several orders of magnitude, consistent with the importance of the electrostatic bond between the lysine and the aldehyde of octanal. When an alanine was substituted for aspartate 204 (D204A), affinity increased over two orders of magnitude, which resulted from the removal of repulsive influences from the aspartate. This effect was also seen when octanoic acid was docked in the D204A mutant receptor model: relative affinity rose from 0.005 in the wildtype to 5 in the mutant. We note that removal of the aspartate would be expected to destabilize the Schiff base we have postulated (see above), which would have unpredictable consequences.

**Table 5** Residue substitution results

| Mutation | Ligand | Ligand class | Predicted relative affinity |
|---|---|---|---|
| OR-I7 K164A | *n*-octanal | aldehyde | <0.0001 |
| OR-I7 D204A | *n*-octanal | aldehyde | 500 |
| OR-I7 D204A | *n*-octanoic acid | carboxylate | 5 |
| OR-I7 V206I | *n*-octanal | aldehyde | 1 |

These lysine 164 and aspartate 204 mutations provided critical tests of the model's ability to simulate site-directed mutagenesis studies. Building on these results, we wished to study valine 206. After Zhao *et al.* (Zhao *et al*., 1998) established that rat OR-I7 responded preferentially to octanal, Krautwurst *et al*. (Krautwurst *et al*., 1998) reported that the closely related mouse OR-I7 preferred heptanal (C7) instead of octanal. They further reported that by mutating residue 206 from valine (rat OR-I7) to isoleucine (mouse OR-I7) they modulated receptor preference from octanal to heptanal; no control on the wildtype rat OR-I7 was presented. Krautwurst *et al*. (Krautwurst *et al*., 1998) hypothesized that an obvious interpretation of these results is that residue 206 contacts the terminal hydrocarbon portion of octanal or heptanal, and that the one-carbon difference between valine and isoleucine complements the one-carbon difference between octanal and heptanal.

Because Krautwurst *et al*. did not test responses in the wildtype rat OR-I7, the OR-I7 model cannot be properly applied to study the mutant effects. However, there is one problem we can address: whether the effect is mediated by

residue 206 inside or outside of the binding pocket. Based on the structure prediction methods used to model OR-I7, as well as comparison with structural information from the BAR, it appears that residue 206 points toward the membrane rather than into the binding pocket (Figure 1).

Hydrophobicity moments for four sets of olfactory receptor sequences ($n$ = 45; see Figure 1), as well as coordinate transfer from with the rhodopsin model of Baldwin *et al.* (Baldwin *et al.*, 1997), independently predict that valine 206 is rotated toward the membrane. Pilpel and Lancet (Pilpel and Lancet, 1999) recently predicted α-helical orientations of olfactory receptors based on sequence variability and found the same rotation. Experimental evidence from the BAR also supports the rotation used for OR-I7 TM5, whose sequence can be aligned definitively with the BAR. Site-directed mutagenesis in the BAR has shown that epinephrine forms H-bonds with two serine residues in TM5 (Strader *et al.*, 1989). To form these bonds the serines must point into the receptor cleft. The serines, shown as open arrows (3) and (4) in Figure 1, correspond to residues 208 and 211 in OR-I7. If these residues face into the receptor cleft, then α-helical structure requires that residue 206 point in the opposite direction, 200° counterclockwise from residue 208 and 140° clockwise from residue 211, as viewed from the extracellular side. Consistent with the disposal of valine 206 towards the membrane in our model, predicted octanal affinity was not influenced by substitution with isoleucine (V206I). This does not imply that the V206I mutation does not exert an indirect effect on octanal and heptanal affinities, a hypothesis that our model cannot simulate. We discuss this hypothesis in more detail below and use the model to propose site-directed mutations as critical tests of this hypothesis.

## Discussion

We have built a molecular model of OR-I7 based on the 7.5 Å map of rhodopsin (Schertler, 1998), hydrophobicity profiles and hydrophobicity moments (Donnelly *et al.*, 1994). As seen in other recent rhodopsin-based GPCR models (Rivkees *et al.*, 1999; Salminen *et al.*, 1999) the structure compared favorably with previous experimental data from rhodopsin, BAR and other GPCRs.

### The octanal binding site of OR-I7

Automatic docking of octanal (see Materials and methods) predicted a binding pocket ~10 Å from the extracellular surface, formed by residues from TMs 3–7. The residue with the most affinity for octanal—lysine 164—formed an electrostatic interaction with the carbonyl oxygen of octanal. Substitution of this lysine with an alanine (K164A) substantially reduced octanal affinity in the OR-I7 model. Aspartate 204 formed an important repulsive interaction with octanal, and alanine substitution of this residue in the model (D204A) increased octanal affinity by over two orders of magnitude. Five hydrophobic residues in TM5, TM6 and TM7 formed Van der Waals interactions with octanal. Mutations in some of these residues would be expected to modulate the carbon chain preferences of OR-I7; others may shield lysine 164 and aspartate 204 from the hydrophobic transmembrane milieu.

### Comparison with the OR5 model and other computational studies

The key residue in this model, lysine 164 (consensus number 430), corresponds in location to a histidine in several mammalian olfactory receptors. This histidine has been predicted to bind odor ligands by three independent olfactory receptor molecular models (Singer and Shepherd, 1994; Bajgrowicz and Broger, 1995; Pilpel and Lancet, 1999). Both the histidine and lysine can exist as positively charged residues and may readily interact with aldehydes. CMA of OR-I7 and other rat olfactory receptors also identified the histidine or lysine position (consensus 430) as one likely to interact with odor ligands (Singer *et al.*, 1995). In other sequence analysis, Ngai *et al.* (Ngai *et al.*, 1993) demonstrated positive Darwinian selection in TM4 of catfish olfactory receptors and argued that it reflects a role in odor binding; inspection of the nucleic acid sequences shows that the positively selected diversity is prominent in the same codon where lysine 164 is found in OR-I7. Together, these results provide several lines of converging evidence for the importance of the lysine 164 in the OR-I7 odor-binding pocket.

Aspartate 204 (consensus position 509), the second most important residue for binding octanal, was predicted as an odor-binding residue by CMA (Singer *et al.*, 1995). This position has already been shown to be critical for acetylcholine binding in the $m_3$ muscarinic receptor (Wess *et al.*, 1991). Phenylalanine 262 (consensus position 633) was also identified by CMA, but was considered at that time as too superficial to participate in the ligand-binding pocket (Singer *et al.*, 1995). The OR-I7 model provides evidence that this residue may also participate in the binding pocket. The alanine 208 site (consensus position 513) was previously identified in our molecular model of OR5 (Singer and Shepherd, 1994). This residue occupies the same position as one of two critical serines in BAR (Strader *et al.*, 1989). The remaining residues, phenylalanine 205, phenylalanine 258 and leucine 281, were unique to the OR-I7 model.

The spatial overlap between predicted binding pockets in the OR5 and OR-I7 models is consistent with the hypothesis that the location of the odor binding pocket is conserved in different receptors, and that functional diversity arises from amino acid substitutions in the pocket (Singer *et al.*, 1995; Pilpel and Lancet, 1999). This phenomenon is known to occur in the family of cationic amine GPCRs (Schwartz *et al.*, 1994).

### Application of the model to elucidate molecular mechanisms: valine 206

The OR-I7 model shows valine 206 pointing away from the binding pocket and into the membrane, yet Krautwurst *et al.* (Krautwurst *et al.*, 1998) report that substitutions in residue 206 modulate OR-I7 quantitative preferences for octanal and heptanal. We hypothesize that these substitutions in residue 206 induce subtle movements in nearby binding pocket residues such as aspartate 204 or phenylalanine 205. A small steric effect, even if <0.5 Å, could cause quantitative shifts in ligand preference from octanal to heptanal. Site-directed mutant experiments in the BAR have already demonstrated that residues outside the binding pocket can have subtle influences on ligand binding (O'Dowd *et al*., 1988; Fraser, 1989; Dohlman *et al*., 1990; Moffett *et al*., 1993; Green *et al*., 1994). Because residue 206 is predicted to point into the membrane, the outcome of substitutions probably depends on nearby lipid molecules or associated receptor molecules. There is now considerable evidence that other GPCRs function as dimers (Jones *et al*., 1998; Kaupmann *et al*., 1998; Kuner *et al*., 1998; White *et al*., 1998). Under these circumstances the V206I mutation may induce steric repulsion at the dimer interface, and thereby force structural chances in the binding pocket.

Current limitations on computer speed and forcefield descriptions do not allow us to simulate the membrane or receptor dimers. The model, however, suggests three mutation experiments to clarify the rotation of TM5 and the effects of the V206I mutation. First, if valine 206 forms direct contacts with the terminal methyl group of octanal, the space created by an alanine mutation (V206A) should shift the preference of OR-I7 from octanal (C8) to nonanal (C9) or decanal (C10). The model predicts that this outcome will not be seen. Second, if valine 206 forms direct contacts with the terminal methyl group of octanal, it should be possible to mutate the valine to a serine and switch OR-I7 preference from octanal to 8-hydroxyoctanal, an analog that could form a hydrogen bond with the newly introduced serine. The model further predicts that this outcome will not be seen. Finally, the OR-I7 model does predict that mutation of aspartate 204 will influence octanal affinity; if this case is confirmed it will help to establish the rotation of TM5. Mutations in other olfactory receptors should also help to resolve this question, as we expect the helical rotation to be conserved across mammalian olfactory receptors.

In summary, we have built a rhodopsin-based molecular model of OR-I7 and automatically docked octanal and related compounds into the model. The results were consistent with functional studies in that octanal had the best affinity for rat OR-I7. The octanal binding pocket consisted of residues from TMs 4–7 and occupied the same location as the epinephrine binding pocket of the BAR. Lysine 164 and aspartate 204 were critical residues in the pocket. We propose that mutation of these residues will affect the affinity of OR-I7 for octanal. We further hypothesize that substitutions in these amino acids in other olfactory receptors confer different odor ligand preferences. Valine 206 did not form contacts with octanal in the model, but other mechanisms may explain how this residue modulates receptor preference for octanal or heptanal. Several analogs of octanal were tested in the model, and their predicted affinities corresponded well with experimental results (Krautwurst *et al*., 1998; Zhao *et al*., 1998). The model may therefore be useful in predicting affinities for ligands not yet tested, as we have reported here for 1-fluoro-*n*-octane. The methods described here can be applied to model other GPCRs of interest. The OR-I7 model will be helpful in generating further insights as experiments on this and other olfactory receptors proceed.

### PDB deposition

Coordinates for the OR-I7-octanal model have been deposited with the Protein Data Bank.

## Acknowledgements

I am grateful to Gordon Shepherd for his guidance and comments on the manuscript, to Wely Brasil Floriano and Vaidehi Nagarajan for consultation on the bacteriorhodopsin model, and to Øyvind Edvarsen for information on BAR mutants. Dan Donnelly provided the PERSCAN software used in this study, and Gerrit Vriend provided WHAT IF. I wish to thank Stuart Firestein and Randall Reed for valuable discussions. MSS is supported by the Yale University MSTP and a National Library of Medicine IAIMS fellowship (awarded to the Yale Center for Medical Informatics, Perry Miller). This work was supported by grants to Gordon M. Shepherd from NICDD; NIDCD, NIA, NASA and NIMH (Human Brain Project); and the DOD-ARO (Multidisciplinary University Research Initiative).

## References

**Bajgrowicz, J.** and **Broger, C.** (1995) *Molecular modelling in design of new odorants; scope and limitations*. In Baser, K.H.C. (ed.), Flavours, Fragrances and Essential Oils. AREP, Istanbul.

**Baldwin, J.M., Schertler, G.F.** and **Unger, V.M.** (1997) *An alpha-carbon template for the transmembrane helices in the rhodopsin family of G-protein-coupled receptors*. J. Mol. Biol., 272, 144–164.

**Buck, L.** and **Axel, R.** (1991) *A novel multigene family may encode odorant receptors: a molecular basis for odorant recognition*. Cell, 65, 175–187.

**Chothia, C., Levitt, M.** and **Richardson, D.** (1977) *Structure of proteins: packing of alpha-helices and pleated sheets*. Proc. Natl Acad. Sci. USA, 74, 4130–4134.

**Cronet, P., Sander, C.** and **Vriend, G.** (1993) *Modeling of transmembrane seven helix bundles*. Protein Engng, 6, 59–64.

**Deisenhofer, J.** and **Michel, H.** (1989) *Nobel lecture. The photosynthetic reaction centre from the purple bacterium* Rhodopseudomonas viridis. EMBO J., 8, 2149–2170.

**Dohlman, H.G., Caron, M.G., DeBlasi, A., Frielle, T.** and **Lefkowitz, R.J.** (1990) *Role of extracellular disulfide-bond cysteines in the ligand*

*binding function of the beta 2-adrenergic receptor*. Biochemistry, 29, 2335–2342.

**Donnelly, D., Overington, J.P.** and **Blundell, T.L.** (1994) *The prediction and orientation of alpha-helices from sequence alignments: the combined use of environment-dependent substitution tables, Fourier transform methods and helix capping rules*. Protein Engng, 7, 645–653.

**Fraser, C.M.** (1989) *Site-directed mutagenesis of beta-adrenergic receptors. Identification of conserved cysteine residues that independently affect ligand-binding and receptor activation.* J. Biol. Chem., 264, 9266–9270.

**Gat, U., Nekrasova, E., Lancet, D.** and **Natochin, M.** (1994) *Olfactory receptor proteins. Expression, characterization and partial purification.* Eur. J. Biochem., 225, 1157–1168.

**Green, S.A., Turki, J., Innis, M.** and **Liggett, S.B.** (1994) *Amino-terminal polymorphisms of the human beta 2-adrenergic receptor impart distinct agonist-promoted regulatory properties*. Biochemistry, 33, 9414–9419.

**Grigorieff, N., Ceska, T.A., Downing, K.H., Baldwin, J.M.** and **Henderson, R.** (1996) *Electron-crystallographic refinement of the structure of bacteriorhodopsin*. *J. Mol. Biol*., 259, 393–421.

**Herzyk, P.** and **Hubbard, R.E.** (1998) *Combined biophysical and biochemical information confirms arrangement of transmembrane helices visible from the three-dimensional map of frog rhodopsin*. J. Mol. Biol., 281, 741–754.

**Issel-Tarver, L.** and **Rine, J.** (1996) *Organization and expression of canine olfactory receptor genes*. Proc. Natl Acad. Sci. USA, 93, 10897–10902.

**Jones, K.A., Borowsky, B., Tamm, J.A., Craig, D.A., Durkin, M.M., Dai, M., Yao, W.J., Johnson, M., Gunwaldsen, C., Huang, L.Y., Tang, C., Shen, Q., Salon, J.A., Morse, K., Laz, T., Smith, K.E., Nagarathnam, D., Noble, S.A., Branchek, T.A.** and **Gerald, C.** (1998) *GABA(B) receptors function as a heteromeric assembly of the subunits GABA(B)R1 and GABA(B)R2*. Nature, 396, 674–679.

**Kaupmann, K., Malitschek, B., Schuler, V., Heid, J., Froestl, W., Beck, P., Mosbacher, J., Bischoff, S., Kulik, A., Shigemoto, R., Karschin, A.** and **Bettler, B.** (1998) *GABA(B)-receptor subtypes assemble into functional heteromeric complexes*. Nature, 396, 683–687.

**Krautwurst, D., Yau, K.W.** and **Reed, R.R.** (1998) *Identification of ligands for olfactory receptors by functional expression of a receptor library*. Cell, 95, 917–926.

**Kuner, R., Kohr, G., Grunewald, S., Eisenhardt, G., Bach, A.** and **Kornau, H.C.** (1998) *Role of heteromer formation in GABAB receptor function.* Science, 283, 74–77.

**Moffett, S., Mouillac, B., Bonin, H.** and **Bouvier, M.** (1993) *Altered phosphorylation and desensitization patterns of a human beta 2-adrenergic receptor lacking the palmitoylated Cys341*. EMBO J., 12, 34–356.

**Nakayama, T.A.** and **Khorana, H.G.** (1991) *Mapping of the amino acids in membrane-embedded helices that interact with the retinal chromophore in bovine rhodopsin*. J. Biol. Chem., 266, 4269–4275.

**Ngai, J., Dowling, M.M., Buck, L., Axel, R.** and **Chess, A.** (1993) *The family of genes encoding odorant receptors in the channel catfish*. Cell, 72, 657–666.

**O'Dowd, B.F., Hnatowich, M., Regan, J.W., Leader, W.M., Caron, M.G.** and **Lefkowitz, R.J.** (1988) *Site-directed mutagenesis of the cytoplasmic domains of the human beta2-adrenergic receptor. Localization of regions involved in G protein-receptor coupling*. J. Biol. Chem., 263, 15985–15992.

**Parmentier, M., Libert, F., Schurmans, S., Schiffmann, S., Lefort, A., Eggerickx, D., Ledent, C., Mollereau, C., Gerard, C., Perret, J. *et al*.** (1992) *Expression of members of the putative olfactory receptor gene family in mammalian germ cells*. Nature, 355, 453–455.

**Pilpel, Y.** and **Lancet, D.** (1999) *The variable and conserved interfaces of modeled olfactory receptor proteins*. Protein Sci., 8, 69–77.

**Ponder, J.W.** and **Richards, F.M.** (1987) *Tertiary templates for proteins. Use of packing criteria in the enumeration of allowed sequences for different structural classes*. J. Mol. Biol., 193, 775–791.

**Popot, J.L.** and **Engelman, D.M.** (1990) *Membrane protein folding and oligomerization: the two-stage model*. Biochemistry, 29, 4031–4037.

**Raming, K., Krieger, J., Strotmann, J., Boekhoff, I., Kubick, S., Baumstark, C.** and **Breer, H.** (1993) *Cloning and expression of odorant receptors*. Nature 361, 353–356.

**Rivkees, S.A., Barbhaiya, H.** and **IJzerman, A.P.** (1999) *Identification of the adenine binding site of the human A1 adenosine receptor*. J. Biol. Chem., 274, 3617–3621.

**Sakmar, T.P., Franke, R.R.** and **Khorana, H.G.** (1989) *Glutamic acid-113 serves as the retinylidene Schiff base counterion in bovine rhodopsin*. Proc. Natl Acad. Sci. USA, 86, 8309–8313.

**Salminen, T., Varis, M., Nyronen, T., Pihlavisto, M., Hoffren, A.M., Lonnberg, T., Marjamaki, A., Frang, H., Savola, J.M., Scheinin, M.** and **Johnson, M.S.** (1999) *Three-dimensional models of alpha(2A)-adrenergic receptor complexes provide a structural explanation for ligand binding*. J. Biol. Chem., 274, 23405–23413.

**Sander, C.** and **Schneider, R.** (1991) *Database of homology-derived protein structures and the structural meaning of sequence alignment*. Proteins, 9, 56–58.

**Schertler, G.F.** (1998) *Structure of rhodopsin*. Eye, 12, 504–510.

**Schwartz, T.W.** (1994) *Locating ligand-binding sites in 7TM receptors by protein engineering*. Curr. Opin. Biotechnol., 5, 434–444.

**Singer, M.S.** and **Shepherd, G.M.** (1994) *Molecular modeling of ligand–receptor interactions in the OR5 olfactory receptor*. NeuroReport, 5, 1297–300.

**Singer, M.S.** and **Shepherd, G.M.** (1997) *Toward a rational structure–function analysis of odour molecules: the olfactory receptor TM4 domain*. In Swift, K.A.D. (ed.), Flavours and Fragrances. Royal Society of Chemistry, Cambridge, pp. 3–10.

**Singer, M.S., Oliveira, L., Vriend, G.** and **Shepherd, G.M.** (1995) *Potential ligand-binding residues in rat olfactory receptors identified by correlated mutation analysis*. Receptors and Channels, 3, 89–95.

**Singer, M.S., Weisinger-Lewin, Y., Lancet, D.** and **Shepherd, G.M.** (1996) *Positive selection moments identify potential functional residues in human olfactory receptors*. Receptors and Channels, 4, 141–147.

**Singer, M.S., Hughes, T.E., Shepherd, G.M.** and **Greer, C.A.** (1998) *Identification of olfactory receptor mRNA sequences from the rat olfactory bulb glomerular layer*. NeuroReport, 9, 3745–3748.

**Stowell, M.H., Mcphillips, T.M., Rees, D.C., Soltis, S.M., Abresch, E.** and **Feher, G.** (1997) *Light-induced structural changes in photosynthetic reaction center: implications for mechanisms of electron–proton transfer*. Science, 276, 812–816.

**Strader, C.D., Sigal, I.S.** and **Dixon, R.A.F.** (1989) *Structural basis of beta-adrenergic receptor function*. FASEB J., 3, 1825–1832.

**Vriend, G.** (1990) *WHAT IF: a molecular modeling and drug design program*. J. Mol. Graph., 8, 52–56.

**Wess, J., Gdula, D.** and **Brann, M.** (1991) *Site-directed mutagenesis of the m3 muscarinic receptor: identification of a series of threonine and*

*tyrosine residues involved in agonist but not antagonist binding*. EMBO J., 10, 3729–3734.

**White, J.H., Wise, A., Main, M.J., Green, A., Fraser, N.J., Disney, G.H., Barnes, A.A., Emson, P., Foord, S.M.** and **Marshall, F.H.** (1998) *Heterodimerization is required for the formation of a functional GABA(B) receptor*. Nature, 396, 679–682.

**Zhao, H., Ivic, L., Otaki, J.M., Hashimoto, M., Mikoshiba, K.** and **Firestein, S.** (1998) *Functional expression of a mammalian odorant receptor*. Science, 279, 237–242.

*Accepted November 1, 1999*